Construction and validation of a novel algorithm based on oncosis-related lncRNAs comprising the immune landscape and prediction of colorectal cancer prognosis

HAOYI XIANG[1,2*], XUNING SHEN[1,2*], ENGENG CHEN[1], WEI CHEN[3] and ZHANGFA SONG[1]

[1]Department of Colorectal Surgery, Sir Run Run Shaw Hospital of Zhejiang University, Hangzhou, Zhejiang 310016; [2]Zhejiang University School of Medicine, Hangzhou, Zhejiang 310011; [3]Cancer Institute of Integrated Traditional Chinese and Western Medicine, Zhejiang Academy of Traditional Chinese Medicine, Tongde Hospital of Zhejiang Province, Hangzhou, Zhejiang 310012, P.R. China

Received July 20, 2022; Accepted December 1, 2022

DOI: 10.3892/ol.2022.13650

Abstract. Colorectal cancer (CRC) has high morbidity and mortality, particularly if diagnosed at an advanced stage. Although there have been several studies on CRC, few have investigated the relationship between oncosis and CRC. Thus, the purpose of the present study was to identify oncosis-related long noncoding RNAs (lncRNAs) and to establish a clinical prognostic model. Original data were acquired from The Cancer Genome Atlas database and PubMed. Differentially expressed oncosis-related lncRNAs (DEorlncRNAs) were identified and were subsequently formed into pairs. Next, a series of tests and analyses, including both univariate and multivariate analyses, as well as Lasso and Cox regression analyses, were performed to establish a receiver operating characteristic curve. A cut-off point was subsequently used to divide the samples into groups labelled as high- or low-risk. Thus, a model was established and evaluated in several dimensions. Six pairs of DEorlncRNAs associated with prognosis according to the algorithm were screened out and the CRC cases were divided into high- and low-risk groups. Significant differences between patients in the different risk groups were observed for several traits, including survival outcomes, clinical pathology characteristics, immune cell infiltration status and drug sensitivity. In addition, PCR and flow cytometry were performed to further verify the model. In summary, a new risk model algorithm based on six pairs of DEorlncRNAs in CRC, which does not require specific data regarding the level of gene expression, was established and validated. This algorithm may be used to predict patient prognosis, immune cell infiltration and drug sensitivity.

Correspondence to: Professor Zhangfa Song, Department of Colorectal Surgery, Sir Run Run Shaw Hospital of Zhejiang University, 3 Qingchun East Road, Hangzhou, Zhejiang 310016, P.R. China
E-mail: songzhangfa@zju.edu.cn

Professor Wei Chen, Cancer Institute of Integrated Traditional Chinese and Western Medicine, Zhejiang Academy of Traditional Chinese Medicine, Tongde Hospital of Zhejiang Province, 234 Gucui Road, Hangzhou, Zhejiang 310012, P.R. China
E-mail: viogro@163.com

*Contributed equally

Key words: colorectal cancer, oncosis-related lncRNAs, prognostic signature, The Cancer Genome Atlas, immune, drug sensitivity

Introduction

Globally, the morbidity of colorectal cancer (CRC) ranks third (10.0%) among all cancers, whereas the mortality rate ranks second (9.4%) (1). Over the past decade, both the incidence and death rates of CRC have increased (2). Through decades of progress in the understanding of CRC pathophysiology, multiple treatments have been developed, including endoscopic and surgical local excision, downstaging preoperative radiotherapy, chemotherapy, biologics and immunotherapy. These treatments in conjunction with several new drugs have led to certain improvements in the survival of patients with CRC; however, these changes remain insufficient in the face of an increasingly severe situation (3). There is a continued need to identify more effective and reliable biomarkers, as well as models to further improve individualized therapy.

Oncosis is a type of programmed death referring to the cellular response to injury that occurs prior to cell death (4). Oncosis is accompanied by cellular and organelle swelling, as well as increased cell membrane permeability. The mechanism of oncosis is based on the incapacity of certain plasma membrane ion pumps, such as sodium-potassium pump and calcium channel (5,6). Certain cell surface receptors (e.g., PORIMIN) are able to trigger oncosis when activated, which may be caused by substances that interfere with ATP production or that increase plasma membrane permeability (7,8). Several previous studies have suggested that oncosis may represent a vital link in tumorigenesis and tumor progression. For instance, one study has demonstrated that aspirin is able to significantly induce the oncosis of HeLa cells through

reduction of the level of the antiapoptotic protein, Bcl-xl, and may therefore significantly inhibit tumor growth (9). When exposed to sanguinarine, multiple cancer cells experience oncosis (e.g., breast and prostate cancer cells) (4). Inducing the programmed death of drug-resistant cancer cells represents an important research direction for the treatment of tumors. In a previous study, a series of synthesized Ir(III) complexes induced oncosis in A549R cells, a type of drug-resistant cancer cell line (10). Long noncoding RNAs (lncRNAs) are defined as transcripts with a length >200 nucleotides that cannot be translated into protein (11). Previous studies on lncRNA have indicated that the dysregulation of lncRNA expression is common in cancer and most abnormal lncRNAs are specific to a particular type of cancer (12-14). In addition, the level of lncRNA expression is a specific biomarker for several types of cancer (15). Increasing evidence suggests that immunity is related to oncosis in cancer (16-18). Furthermore, interleukin-33 production by cells may enhance programmed oncosis in low-metastatic cells in hypoxic regions in lung cancer (19). LncRNA has an important role in events (e.g., $CD4^+$ T-cell differentiation and T-cell activation) (20) that are essential for immune regulation (21). The prognosis of patients further differs based on differential gene mutations (22).

In cancer diagnostic models, the combination of two biomarkers is more accurate than an individual biomarker (23). Thus, in the present study, a pairing oncosis-related lncRNA (orlncRNA) algorithm was constructed. By obtaining information on the expression of orlncRNA pairs, the corresponding results, including patient prognosis, immune-cell infiltration and drug sensitivity was able to be determined while avoiding common algorithm problems (e.g., data correction in the application process of the model). The presented algorithm provides a novel method by which the clinical outcomes of CRC may be predicted, potentially providing a method of selecting appropriate immunotherapy and chemotherapy treatments.

Materials and methods

Data acquisition. First, the transcriptome data of patients with CRC were downloaded from The Cancer Genome Atlas database (TCGA; https://portal.gdc.cancer.gov/) (24) in November 2021. The transcriptome data were reported as fragments per kilobase per million mapped reads. Next, gene transfer format (GTF) files were applied to distinguish between lncRNA and mRNA. Subsequently, the corresponding clinical data were downloaded and repeated invalid clinical information was deleted. In addition, a list of oncosis-related genes (orgenes) was obtained by searching for 'oncosis cancer' on PubMed (https://pubmed.ncbi.nlm.nih.gov/) (25).

Recognition of differentially expressed orlncRNAs (DEorlncRNAs). OrlncRNAs were screened out by a co-expression analysis and the expression correlation was explored between orgenes and lncRNAs, and the screening criteria for orlncRNAs were established, for which the immune gene correlation coefficient value was >0.4 and the P-value was <0.001. The differential expression of orlncRNAs between cancerous and normal samples was also assessed, all using limma, an R package (version 3.50.0) was used (26). To improve the accuracy, a log fold-change >2 and false discovery rate (FDR) <0.05 was set as the threshold.

Construction of DEorlncRNA pairs. The aforementioned DEorlncRNAs were copied into two empty files, labelled as A and B, and every DEorlncRNAs in file A were cyclically singly paired with all DEorlncRNAs in file B. A 0-1 matrix could be constructed using the following logic: Assume that A represents a pair of DEorlncRNAs, for instance, representing lncRNAB paired with lncRNAC. If the level of lncRNAB expression is higher than that of lncRNAC, A is equal to 1; otherwise, A is equal to 0. If the expression of DEorlncRNA pairs was calculated as either 0 or 1 among a majority (>80%) of all samples, those lncRNA pairs were not adopted in the following prognostic analysis, since there is no certain degree of difference in lncRNA pairs, which means that an accurate prediction of patient survival is impossible. Only the DEorlncRNA pairs with an expression of 0 or 1 in 20-80% of all samples were considered valid.

Construction of the risk assessment model. Univariate Cox analysis was first performed on DEorlncRNA pairs, after which a Lasso regression with 10-fold cross validation was performed with a threshold P-value of 0.05. A total of 1,000 cycles were performed in the Lasso regression to minimize the cross-validation error in obtaining the DEorlncRNA pairs. The pairs were subsequently used in the Cox proportional hazards regression analysis and the model analysis was then carried out. The akaike information criterion (AIC; AIC=-2log L+2V, where L is the maximum likelihood of a fit model and V is the number of free parameters) was calculated for each model (27) and was applied in the following steps. The AIC of each model was calculated, which was then aborted once the AIC value reached the minimum point, and that model was recognized as the optimal candidate model. Next, the receiver operating characteristic (ROC) curves for 1, 3 and 5 year survival were plotted. The following formula was used to calculate the risk score for all samples:

$$\text{Risk Score} = \sum_{i=1}^{n} \text{Coef (i)x E(i)}$$

Coef (Table I) represents the coefficient from the multivariate Cox regression analysis of each DEorlncRNA pair and E represents the expression value of the DEorlncRNA pairs, which was obtained during the aforementioned recognition of DEorlncRNAs. Each point on the ROC curve was evaluated to obtain the sum of sensitivity and specificity. The high- or low-risk scores were divided by the cut-off value, which was equal to the risk score obtained from the maximum point of the curve. The survival (version 3.2-13), survminer (version 0.4.9), survivalROC (version 1.0.3) and glmnet (version 4.1-3) R packages were used in the above steps.

Verification of the constructed model using all 548 cases from TCGA. The cut-off point used was first verified. Kaplan-Meier analysis was used to indicate the survival differences between groups with different risk grades through the log-rank test and the curve was plotted for visualization. The R tool was used to visualize the specific risk score of each sample in the model.

To explore the clinical value of the model, a χ^2 test was performed to analyze the relationship between the model and different clinical traits (e.g., patient age, sex and American

Table I. Regression coefficients of DEorlnRNAs included in the Lasso regression analysis.

DEorlncRNA	Coefficient
SCAT2|AC112496.1	0.79067414
ARHGEF38-IT1|AL136115.2	-0.62254692
AC026356.1|AC026368.1	0.56929575
AC016831.4|AC104695.4	-0.90749403
AC092338.1|AC087222.1	0.67053059
LINC01811|MIR181A2HG	-0.36402154

DEorlncRNA, differentially expressed oncosis-related lncRNAs.

Joint Committee on Cancer tumor stage) (28). The results of the analyses were displayed in a band diagram that was subsequently plotted. A Wilcoxon signed-rank test was applied to calculate the difference in the risk scores among groups with different clinicopathological features (e.g., patient age, sex and tumor stage). The results of the analyses were presented as a box-plot. Cox regression analysis, including single and multivariate variables, was applied to evaluate the association between the risk score and the aforementioned clinicopathological features. Thus, whether the risk model may be an independent prognostic indicator of CRC was verified. The results were displayed in a forest map. The R packages survival, surviviner, survivalROC, limma, ggpubr, pheatmap and complex Heatmap were used for the aforementioned analyses.

Gene association analysis based on risk score. To explore the differences in gene expression between the high and low-risk groups, the level of target gene expression and patients' risk score values were first extracted and then combined. Next, the data were compared between the two groups. The mean values used for testing were compared and the results of the analysis were presented in a violin diagram. The limma and ggpubr R packages were used for this analysis. Gene expression status was verified through using the immunohistochemical staining database (accession no. CAB013272, CAB013272, CAB000003, CAB004022, CAB011671, CAB025583 and HPA003590; https://www.proteinatlas.org/).

Correlation analysis with tumor-infiltrating immune cells. Since the lncRNAs recognized by the co-expression analysis were initially associated with orgenes (and therefore may also be linked to immunity), the correlation of the model related to immune cell infiltration in the tumor microenvironment was investigated. To investigate the potential connection between the risk score and tumor-infiltrating immune cells, a method that combined currently acknowledged methods of evaluating the immune cell infiltration status among CRC samples was applied, which included XCELL, TIMER, QUANTISEQ, MCPCOUNTER, EPIC, CIBERSORT-ABS and CIBERSORT. To improve the accuracy of the correlation analysis, the content of infiltrating immune cells was compared between the aforementioned high- and low-risk groups with a Mann-Whitney U-test. Spearman's correlation analysis was used to analyze the correlation between risk score and immune cell infiltration. The cut-off value was set as $P<0.05$ and these results were presented in a lollipop diagram. The R packages limma, scales, ggplot2 and ggtext were applied as in the aforementioned analyses.

Functional assessment of the model in clinical therapy. To assess the application value of the model in clinical therapy for CRC, the IC_{50} values of several common immunotherapy and chemotherapy drugs in the TCGA dataset were evaluated. Antitumor medication used in this assessment included cisplatin, camptothecin, doxorubicin, dasatinib, bleomycin and docetaxel. The Mann-Whitney U-test was applied to compare the IC_{50} of the drugs between the high- and low-risk groups. Box plots were used to visualize the results. The R packages limma, ggpubr, pRRophetic and ggplot2 were used to complete the aforementioned tests.

Sampling of tumor tissues. A tissue sample with pathological stage T2N0Mx was collected from a male patient with colorectal cancer (aged 55 years) in January 2022 at Sir Run Run Shaw Hospital (Hangzhou, China). The tumor tissue was placed in Tissue RNA protection solution RNAsafer Stabilizer Reagent (cat. no. R1100; Applygen Technologies, Inc.) and stored at -80˚C. Prior to sampling, the surface of the tumor was thoroughly cleaned with PBS to remove any impurities from the surface of the tumor. The tumor was then cut open and ~100 mg of the brittle part of the center of the tumor was taken as the experimental sample.

Verification by reverse transcription-quantitative PCR (RT-qPCR). TRIzol™ (Invitrogen; Thermo Fisher Scientific, Inc.) was used to extract total RNA from the CRC tissues as per the manufacturer's instructions. A NanoDrop™ 2000 Spectrophotometer (Thermo Fisher Scientific, Inc.) was used for RNA quantification, with the A260/280 ratio indicating RNA purity. RT was performed using the PrimeScript RT Reagent Kit according to the manufacturer's protocol (Takara Biotechnology Co., Inc.). Then cDNA amplification was performed on a C1000 Touch Thermal Cycler Detection System (Bio-Rad Laboratories, Inc.) in triplicate. The reaction mixture (total volume, 50 μl) was comprised of 1 ng cDNA, 125 nM forward and reverse primers and 25 μl 2X SYBR® Premix Ex Taq™ (Takara Biotechnology Co., Inc.). The thermocycling conditions were as follows: Initial denaturation at 95˚C for 1 min, followed by 42 cycles of 95˚C for 15 sec, 56˚C for 25 sec and 72˚C for 30 sec. The primers used are listed in Table SI. lncRNA expression levels were assessed using the cycle threshold method according to the according to previously reported methods (29). The lncRNA expression levels were analyzed using an unpaired Student's t-test. Expression levels were compared according to the cycle threshold values of each selected DEorlncRNA, which were then verified for each sample according to the aforementioned risk score formula.

Verification of the biological impact of the orlncRNAs. LoVo CRC cell lines were purchased from the American Type Culture Collection. LoVo cells were maintained in 1640 (HyClone; Cytiva) with 10% FBS (Gibco; Thermo Fisher Scientific, Inc.) and 100 U/ml penicillin. LoVo cells

were seeded into a 6-well plate and cultured at 37˚C and 5% CO_2. Their growth was closely monitored until they reached 80% confluence, and they were then transfected with siRNA (siRNA Transfection Reagent; cat. no. sc-29528; Santa Cruz Biotechnology, Inc.) using Lipofectamine 2000 (Invitrogen; Thermo Fisher Scientific, Inc.). Briefly, Lipofectamine 2000™ was diluted to 5 μl/well and siRNA were diluted to a final concentration of 100 nM. The solutions were incubated separately for 5 min and mixed for 15 min, both at 25C. The mixture was then added to the cells in the 6-well plate and incubated at 37C. After 8 h, the growth medium was changed to fresh media and the cells were further incubated at 37˚C for 24 h under 5% CO_2. The cells were immediately collected for further analysis.

Oncosis was induced in LoVo cells with or without lncRNA knockdown (30) [using small interfering RNA-MIR181A2 host gene (si-MIR181A2HG) or si-negative control (si-NC); Table SII] with 0.01% Triton X-100 (Sigma-Aldrich; Merck KGaA) (31) for 10 min at 37˚C and repeated 3 times. After induction, the cells were centrifuged at 300 x g for 5 min at 25˚C the supernatant was discarded and the cells were collected. The cells were gently resuspended in PBS and counted using a Countess II fluorescence microscope (Thermo Fisher Scientific, Inc.). A total of $2x10^5$ suspended cells were centrifuged at 300 x g for 5 min and the supernatant was discarded. The cells were washed once more with PBS and the supernatant was discarded after centrifugation. To resuspend the cells, 500 μl DilC1(5) dyeing solution (CAS no. 36536-22-8; Enzo Life Sciences, Inc.) was added to the cell pellet. The cells were then incubated in a 5% CO_2 incubator at 37˚C for 15-20 min. After this incubation, the cells were centrifuged at 300 x g for 5 min, the supernatant was discarded and 500 μl pre-cooled (4˚C) 1X PBS was added to the cells. This cell washing was repeated twice. Finally, 500 μl of the aforementioned precooled buffer was used to resuspend the cells. The samples were stored on ice and detected by flow cytometry within 30 min.

The cell suspensions were analyzed by flow cytometry (BD FACSCalibur; BD Biosciences) and the fluorescence channels corresponding to the dyes were selected for data analysis [DilC1(5) was detected in the 660/20 nm channel on HeNe trigon]. The data were analyzed and processed using FlowJo (version 10.8.1, FlowJo LLC).

For the fluorescence microscope observation, the cells (a total of $2x10^5$) were seeded in a confocal dish for different treatments as 6 groups in the aforementioned flow cytometry section. A total of 200 μl of the DilC1(5) dyeing solution (CAS no. 36536-22-8; Enzo Life Sciences, Inc.) was then added and the cells were incubated at 37˚C with 5% CO_2 for 15-20 min. After incubation, 1X PBS was used to wash the cells 1-2 times. Finally, the coverslip was placed upside down on the slide and the slide was observed under a fluorescence microscope.

Statistical analysis. The R package limma was applied to recognize DEorlncRNAs, and log fold-change >2 and FDR <0.05 was set as the threshold. Univariate Cox analysis, Lasso regression, Cox proportional hazards regression analysis, multivariate Cox regression analysis and R packages (survival, surviviner, survival ROC and glmnet) were used to construct the risk assessment model. The χ^2 test, Wilcoxon signed-rank test, uni- and multivariate Cox regression analyses and R packages (survival, survminer, survival ROC, limma, ggpubr, pheatmap and complex Heatmap) were used to verify the model. The R packages (limma and ggpubr) were used in gene correlation analysis. Mann-Whitney U-test, Spearman's correlation analysis, Wilcoxon signed-rank test and R packages (limma, scales, ggplot2 and ggtext) were used to analyze the association between risk score and immune cell infiltration, and the cut-off value was set as $P<0.05$. The Mann-Whitney U-test and R packages (limma, ggpubr, pRRophetic and ggplot2) were used to complete the assessment of the model in clinical therapy. Experimental data analysis was performed using GraphPad Prism 9.00. $P<0.05$ was considered to indicate statistical significance. All of the individual statistical analyses are elaborated on in the corresponding methods sections.

Results

Recognition of DEorlncRNAs. The process flow of the present study is presented in Fig. 1. First, 44 normal and 568 CRC samples were acquired from the TCGA projects (projects screened for, colon adenocarcinoma and rectum adenocarcinoma). The CRC transcriptome data were also obtained from the TCGA database. Subsequently, a total of 33 oncosis-related genes were collected by screening on PubMed. Next, Ensembl GTF files were used to annotate the data and a co-expression analysis was performed between the orgenes and lncRNA. As many as 357 orlncRNAs were recognized by using R-x64-4.1.2 language. Of these, 48 were recognized as DEorlncRNAs through a differential expression analysis. The heat map in Fig. 2A presents all of the recognized DEorlncRNAs and their expression status. All of these DEorlncRNAs were highly expressed (Fig. 2B).

Construction of the DEorlncRNA pairs and the risk model. By using iterative loop pairing and 0-or-1 matrix screening, 804 valid DEorlncRNA pairs were acquired from 48 DEorlncRNAs. A total of 13 DEorlncRNA pairs associated with prognosis were extracted using univariate analysis. A Lasso regression analysis was applied to prevent over-fitting and nine DEorlncRNA pairs were screened out. Finally, six DEorlncRNA pairs were absorbed into a Cox proportional hazard model by a stepwise method (Fig. 2C). Thus, the risk score for all samples was calculated using the risk score formula and the coefficients (Table I) obtained from the aforementioned process.

Next, the ROC curve of the model was plotted. The area under curve (AUC) of the model was 0.724, which was >0.7 (Fig. 3A). This finding suggests that this model exhibited a fair predictive capability. To confirm the superiority of the model, the 1, 3, and 5-year ROC curves were plotted. The AUC value of every curve shown in the results was >0.7 (Fig. 3B). In addition, the 1-year ROC curve analysis with other clinical features (e.g., age, sex and stage) were also performed and the results indicated that the risk score had a greater AUC value compared with the other indicators (Fig. 3C). The maximum inflection point was recognized by calculating and comparing each point of the ROC curve. A value of 1.207 was recognized as the cut-off value (Fig. 3D). This value was used to separate the samples into different

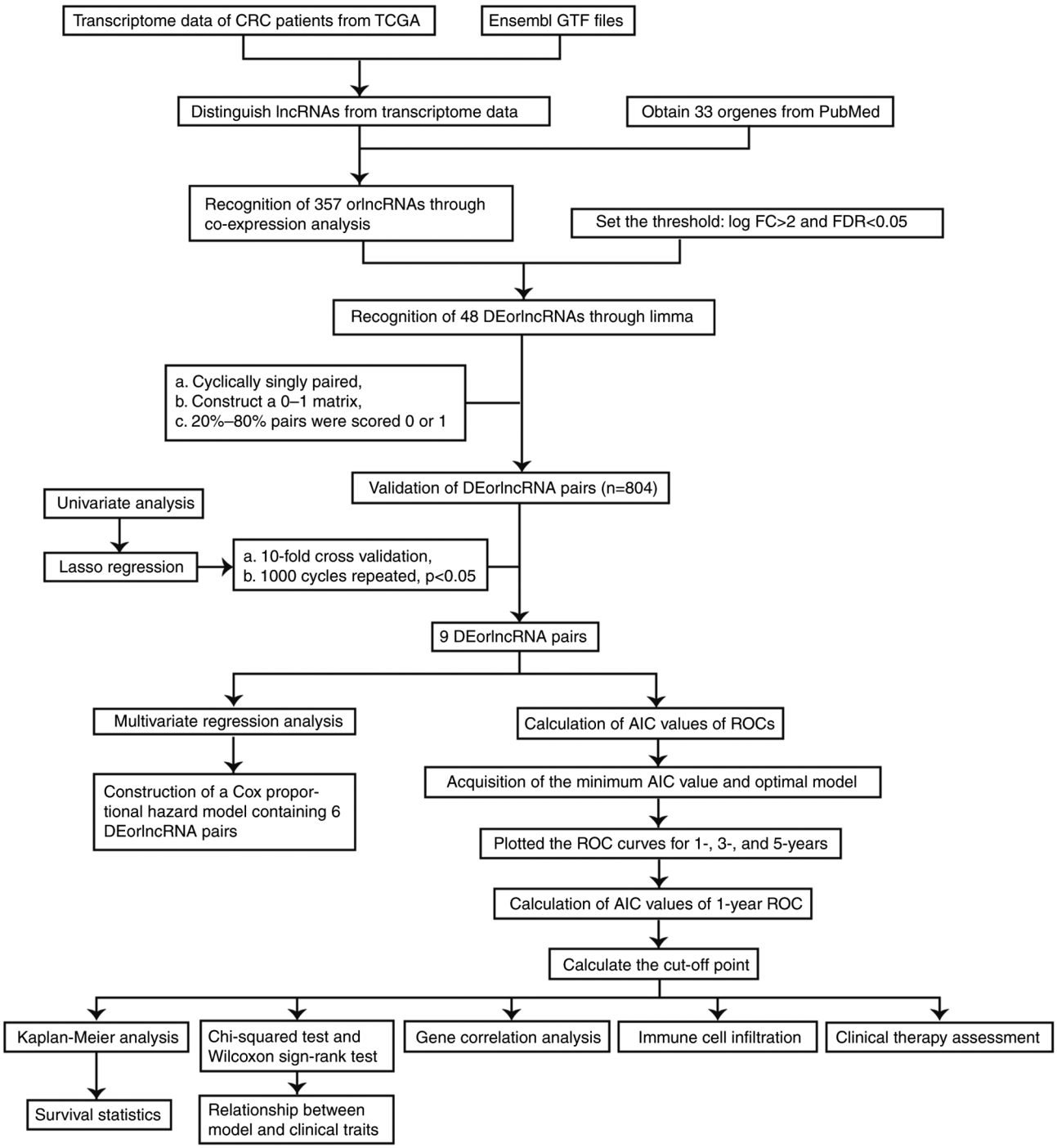

Figure 1. Flow chart of the present study. AIC, akaike information criterion; CRC, colorectal cancer; DEorlncRNA, differentially expressed oncosis-related long noncoding RNA; GTF, gene transfer format; FC, fold change; FDR, false discovery rate; orgenes, oncosis-related genes; ROC, receiver operating characteristic; TCGA, The Cancer Genome Atlas.

risk groups. A total of 548 CRC samples were obtained from TCGA database, and 33 cases were excluded due to including incomplete data. Then the risk score of these rest cases was calculated. Subsequently, for further verification, the samples were re-distinguished and divided into high- and low-risk groups by the cut-off value.

Verification of the constructed model and its application in clinical evaluation. According to the cut-off value, 221 cases were classified into the high-risk group, whereas 294 cases were categorized into the low-risk group. The plots in Fig. 4A and B display the risk scores and survival status of these cases, respectively. These results indicated that the patients' survival rate and survival time were negatively associated with the risk score. As indicated by the Kaplan-Meier survival analysis, the survival time of the patients in the high-risk group was shorter than that of the low-risk group (Fig. 4C).

Subsequently, a strip chart and scatter diagrams indicated that there was a significant association between the risk score and clinical, tumor, metastasis and node stages according to

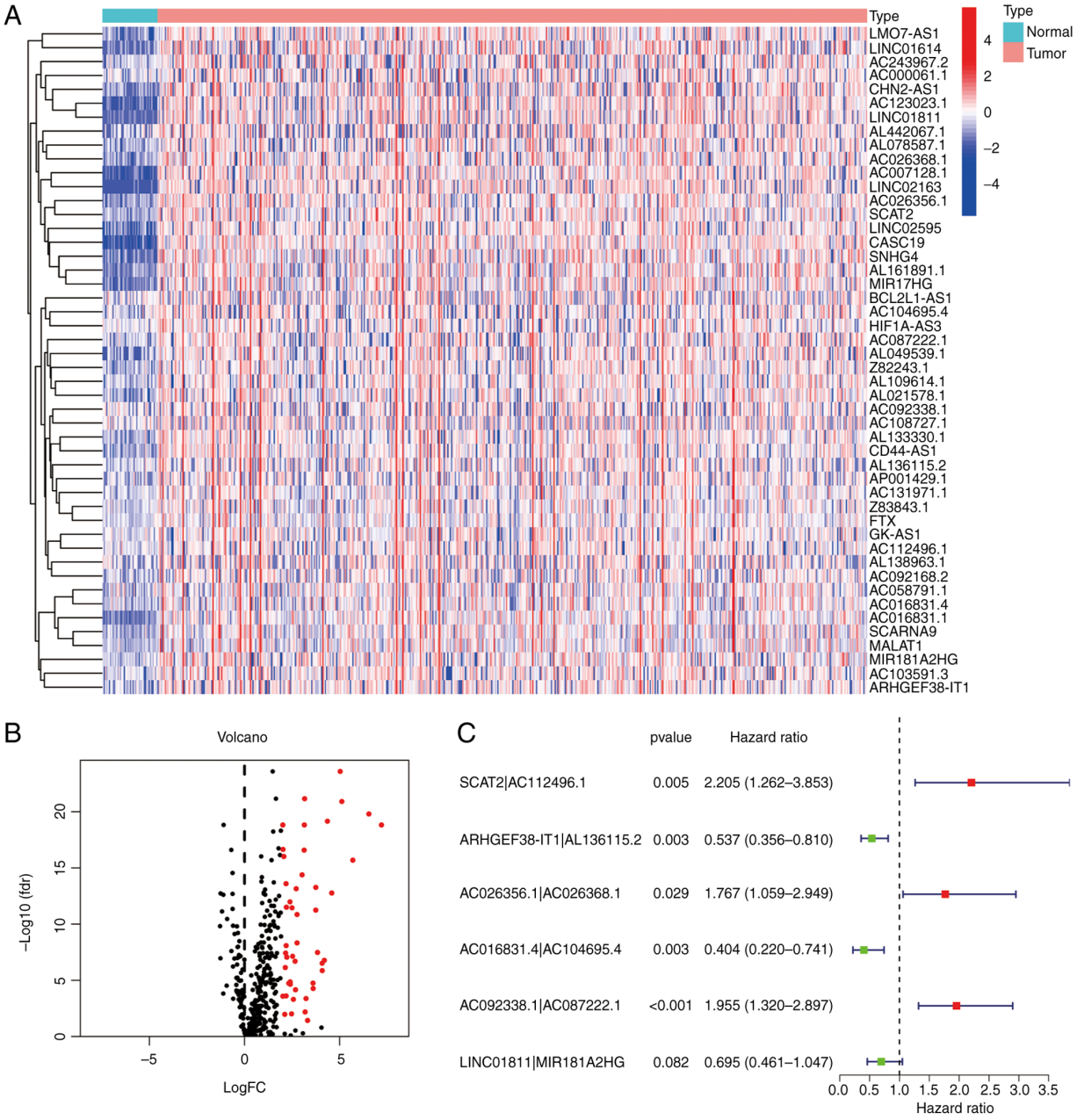

Figure 2. Recognition of DEorlncRNAs. (A) Heatmap and (B) volcano plot displaying the expression of 48 DEorlncRNAs in colorectal cancer and normal samples. The columnar bands from 4 to -4 in figure A represented lncRNA expression levels as calculated using the pheatmap R package. Red points represent highly expressed DEorlncRNAs, and black points represent normally expressed DEorlncRNAs (C) Forest map of the six DEorlncRNA pairs included in the model (AC112496.1, AL136115.2, AC026356.1, AC026368.1, AC016831.4, AC104695.4, AC092338.1 and AC087222.1 are sequence accession numbers). FC, fold change; fdr, false discovery rate; DEorlncRNA, differentially expressed oncosis-related long noncoding RNA.

the results of a Wilcoxon signed-rank test (Fig. 5A-E). Groups displaying an advanced stage were associated with a higher risk score. Univariate Cox regression analysis indicated that age [hazard ratio (HR), 1.031; 95% confidence interval (CI), 1.013-1.051], clinical stage (HR, 2.172; 95% CI, 1.727-2.731) and risk score (HR, 1.595; 95% CI, 1.397-1.823) were statistically significant between the low- and high-risk groups (Fig. 5F). The multivariate Cox regression analysis indicated that age (HR, 1.038; 95% CI, 1.019-1.057), clinical stage (HR, 2.276; 95% CI, 1.797-2.882) and risk score (HR, 1.493; 95% CI, 1.307-1.706) may serve as independent prognostic predictors (Fig. 5G). The P-values for the aforementioned data were all >0.001.

Gene association analysis based on the risk score. The results indicated that a high-risk score was positively associated with genes such as ATG12 (P<0.05), BCL2 (P<0.05), LMNA (P<0.001), SNAI2 (P<0.05) and UCP2 (P<0.01) (Fig. 6A-E), whereas risk was negatively associated with NDRG2 (P<0.05) (Fig. 6F). Immunohistochemical staining images also indicated that the expression levels of ATG12, BCL2, LMNA, SNAI2 and UCP2 were higher in cancer tissue compared with those in normal tissue (Fig. 7).

Analysis of immune cell infiltration. Patients in the high-risk group exhibited a positive association with immune cells, including cancer-associated fibroblasts, macrophages, $CD4^+$ T

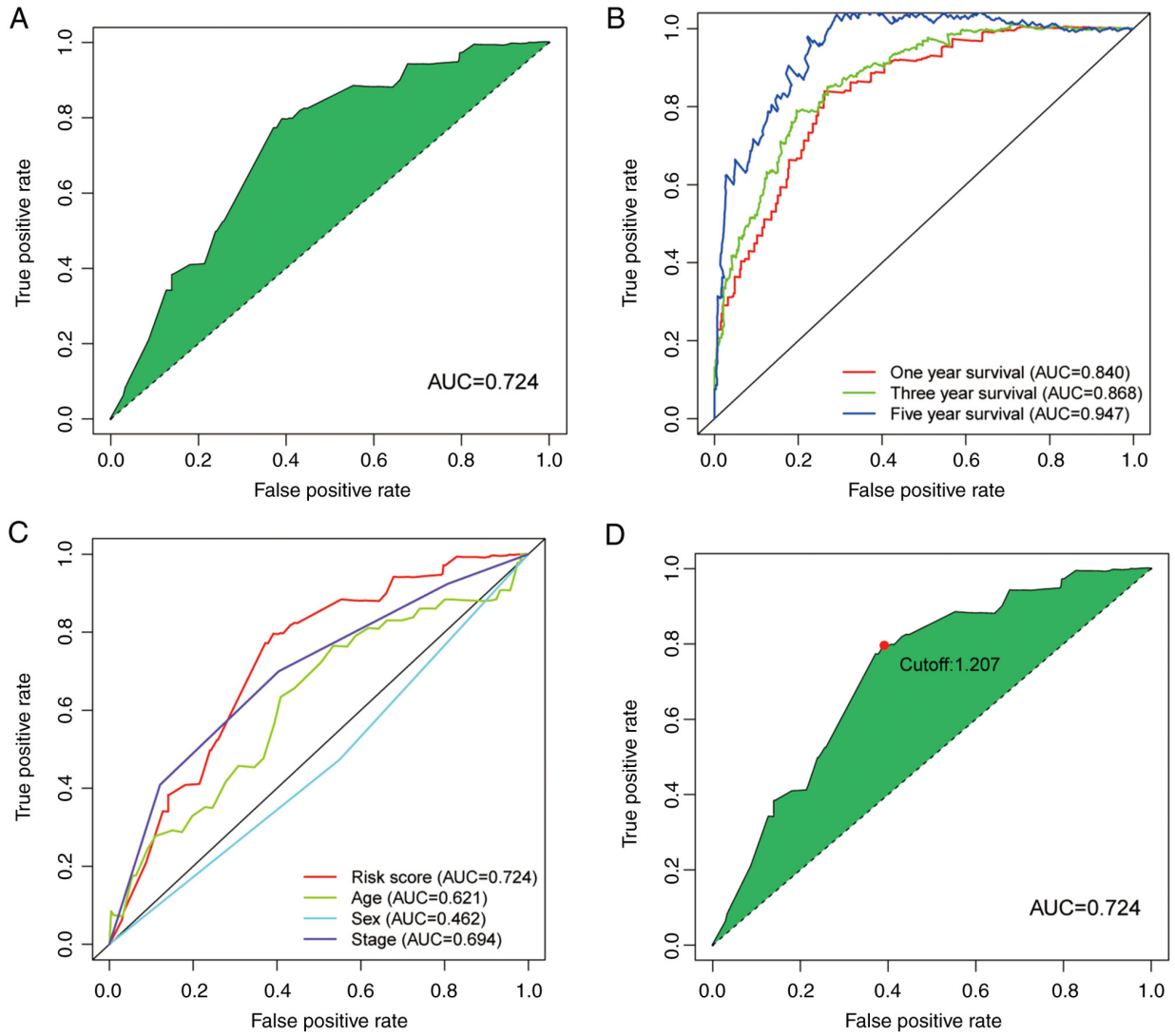

Figure 3. Construction of differentially expressed oncosis-related long noncoding RNA pairs and risk assessment model. (A) ROC curve for survival and AUC value of the model. (B) The 1-, 3- and 5-year survival ROC curves and AUC values. (C) Comparation status between the 1-year ROC curve and other clinical characteristics. (D) A risk score of 1.207 was used as the cut-off value, which was used to distinguish the risk groups of the samples. AUC, area under curve; ROC, receiver operating characteristic.

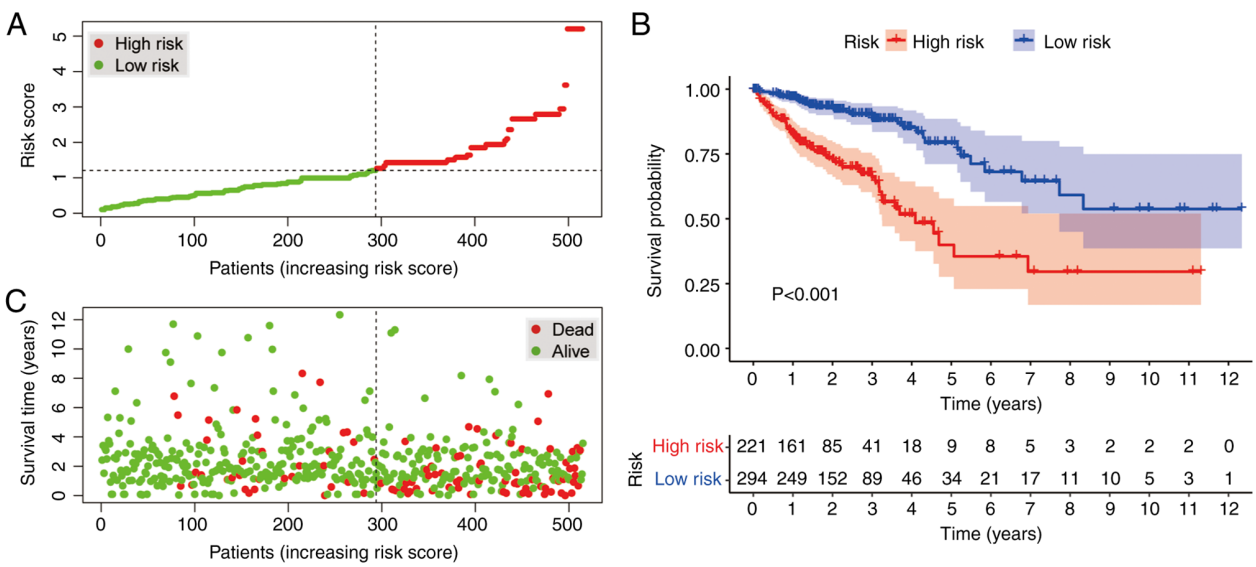

Figure 4. Verification of the constructed model. (A) Visualization of the risk score and (C) survival time/status of each case. (B) Kaplan-Meier analysis of the high- and low-risk groups.

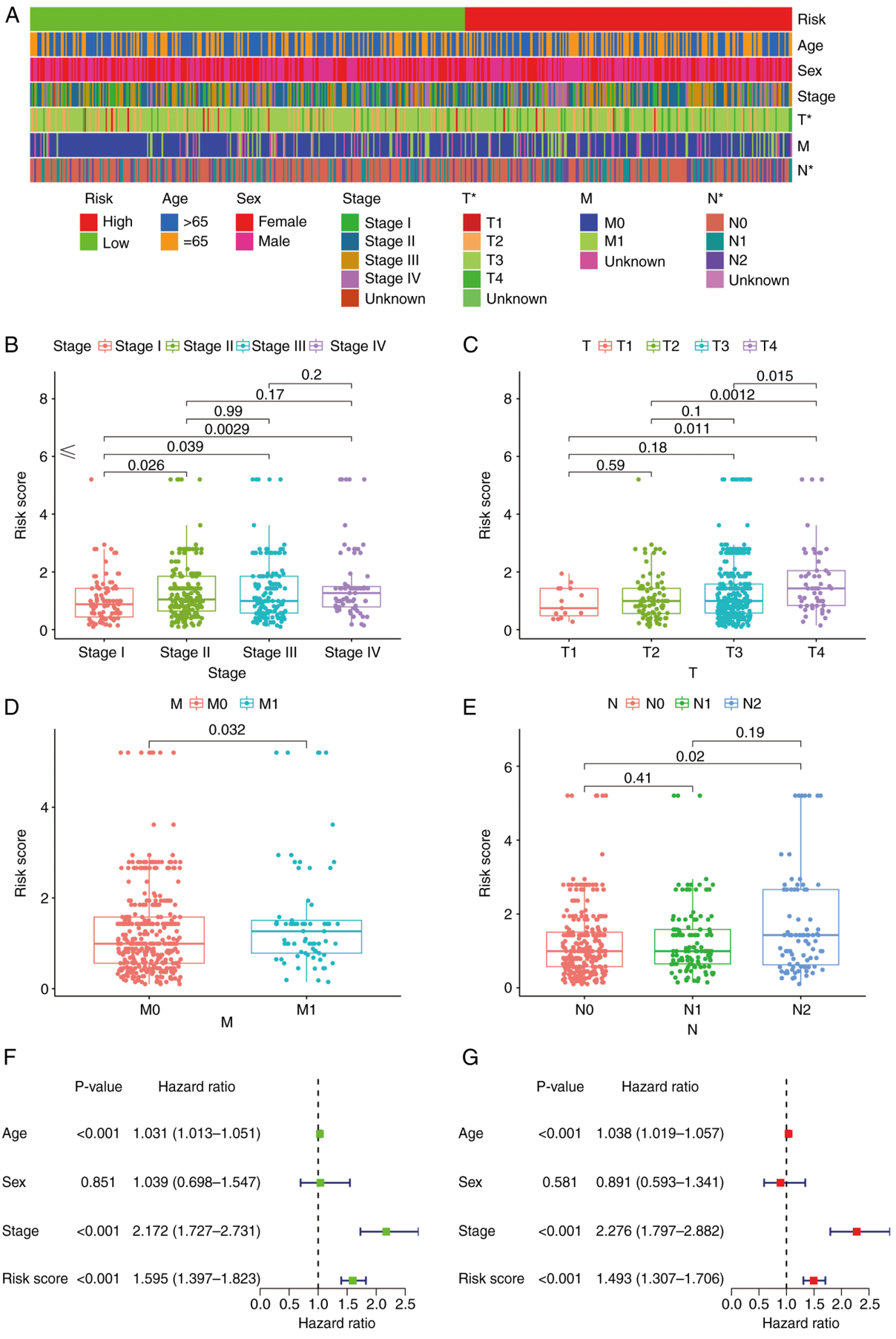

Figure 5. Model application for clinical evaluation. The (A) band diagram and box plots (B-E) showed that clinical, T, M and N stages were significantly associated with risk score, *P<0.05. (F) Univariate Cox regression analysis showed that age, clinical stage and risk score were considered to be statistically significant. (G) Multivariate Cox regression analysis showed that age, clinical stage and risk score were independent prognostic predictors. M, metastasis; N, node; T, tumor.

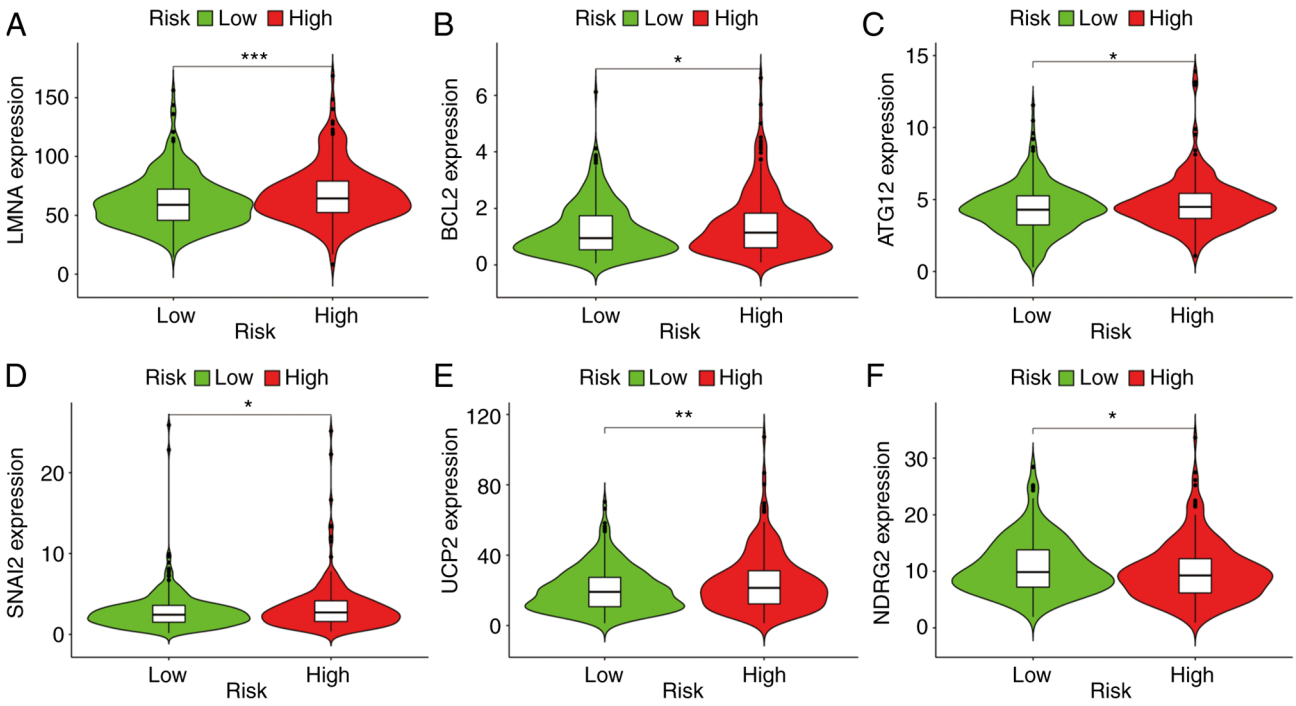

Figure 6. Gene expression analysis based on risk score. (A-E) The levels of (A) LMNA, (B) BCL2, (C) ATG12, (D) SNAI2 and (E) UCP2 expression were higher in the high-risk group than that in the low-risk group. (F) The level of NDRG2 expression was higher in the low-risk group. *P<0.05, **P<0.01 and ***P<0.001.

cells and natural killer (NK) cells (Fig. 8B-E). Using Spearman's correlation analysis, the relationship between risk score and immune-infiltrating cells in multiple databases was displayed in a lollipop chart (Fig. 8A) and the specific values are listed in Table II.

Model functional assessment for clinical therapy. The results indicated that a high-risk score was related to a lower IC_{50} for certain therapeutic medicines, including bleomycin (P=0.003), camptothecin (P=0.00024), dasatinib (P=0.038), docetaxel (P=0.028), doxorubicin (P=0.0017) and cisplatin (P=1.2x10^{-5}) (Fig. 9). This finding suggests that the model has the potential to assist with predicting drug sensitivity.

RT-qPCR. The expression levels of six lncRNA pairs in the patient tumor tissue are presented in Fig. 10. The risk value calculated according to the formula is 0.839, indicating this patient belongs to the low-risk group. The expression level of ATG12, BCL2, LMNA, SNAI2 and UCP2 in CRC tissue and normal tissue is presented in Fig. 11, which indicates that the expression of these genes was higher in the tumor tissue than in normal tissue.

Verification of the biological impact of MIR181A2HG. Through the use of flow cytometry and DilC1(5), it was observed that after oncosis induced by Triton X, the mitochondrial membrane potential of the three groups whose treatment included Triton X decreased (Fig. 12A). The decrease in mitochondrial membrane potential in the MIR181A2HG expression knockdown group was more significant than that in the negative control group. Through the use of fluorescence confocal microscopy, it was seen that DilC1(5) fluorescence decreased in the Triton X-induced groups and DilC1(5) fluorescence decreased more markedly after knockdown of MIR181A2HG expression. Morphologically, compared with the control group, the cells in the Triton treatment group increased in volume and demonstrated swelling. After MIR181A2HG expression was knocked down, the cell oncosis was more apparent, the intracellular structure and membrane appeared blistered, and membrane integrity was damaged (Fig. 12B).

Discussion

Oncosis is a fundamental modality of cell death that may lead to oncotic necrosis and was first discovered in models of ischemic injury (8). Oncosis has an important role in the transition between apoptosis, autophagy and necrosis (32). The relationship between oncosis and tumors has been widely studied. For instance, overexpression of ion channels may induce breast cancer cells to undergo oncosis to promote cell death (6). It has also been found that gastric cancer cell death may be induced by QC4 via oncosis (33). LncRNA also has important implications in numerous aspects of cancer, including proliferation, survival, migration and genomic stability (34). The construction of prognostic markers for predicting the overall survival (including survival rate and time) of patients with cancer using lncRNA has become an area of increased research (35,36). The survival outcome, immunotherapy effect and drug sensitivity of patients with cancer may be determined by detecting the expression status of several lncRNAs, such as AC016027.1, AC099850.3 and ELFN1.AS1, which may provide clinical diagnosis and treatment options (35,37,38). Certain studies have focused on the construction of autophagy, immune and other coding genes, as well as non-coding RNA models to

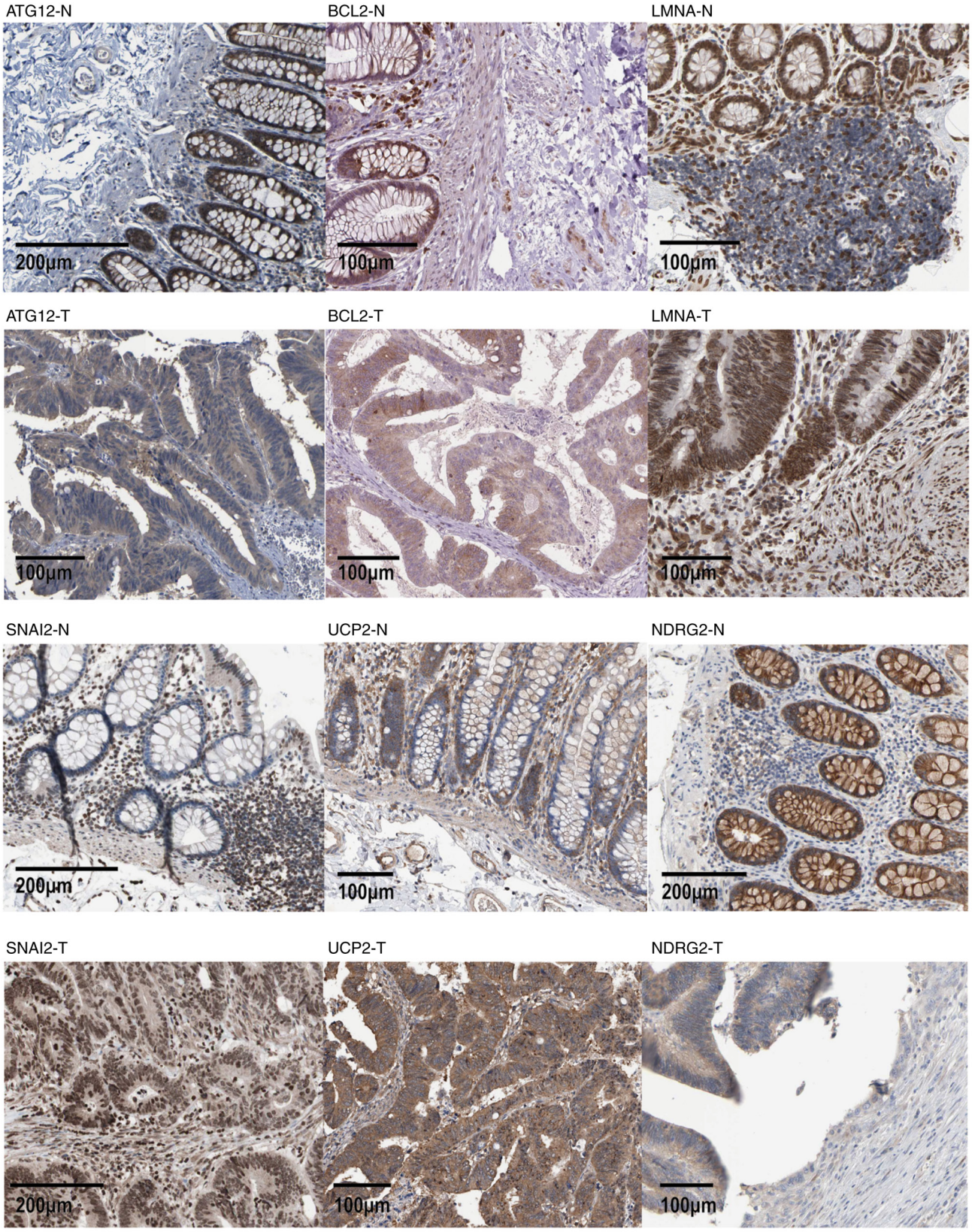

Figure 7. Immunohistochemical staining status of critical genes in normal tissue and colorectal cancer tissue from the same patient. N, normal tissue; T, colorectal cancer tissue.

predict the prognosis of CRC (35,39). However, to the best of our knowledge, there are no studies to date that have established an orlncRNA model to evaluate CRC-related traits. The present study built on previous research that has been using a reasonable scheme composed of paired DEorlncRNAs (40), effectively reducing the complex data batch correction and achieving a more accurate risk assessment and CRC prognosis prediction while reducing the data required for this.

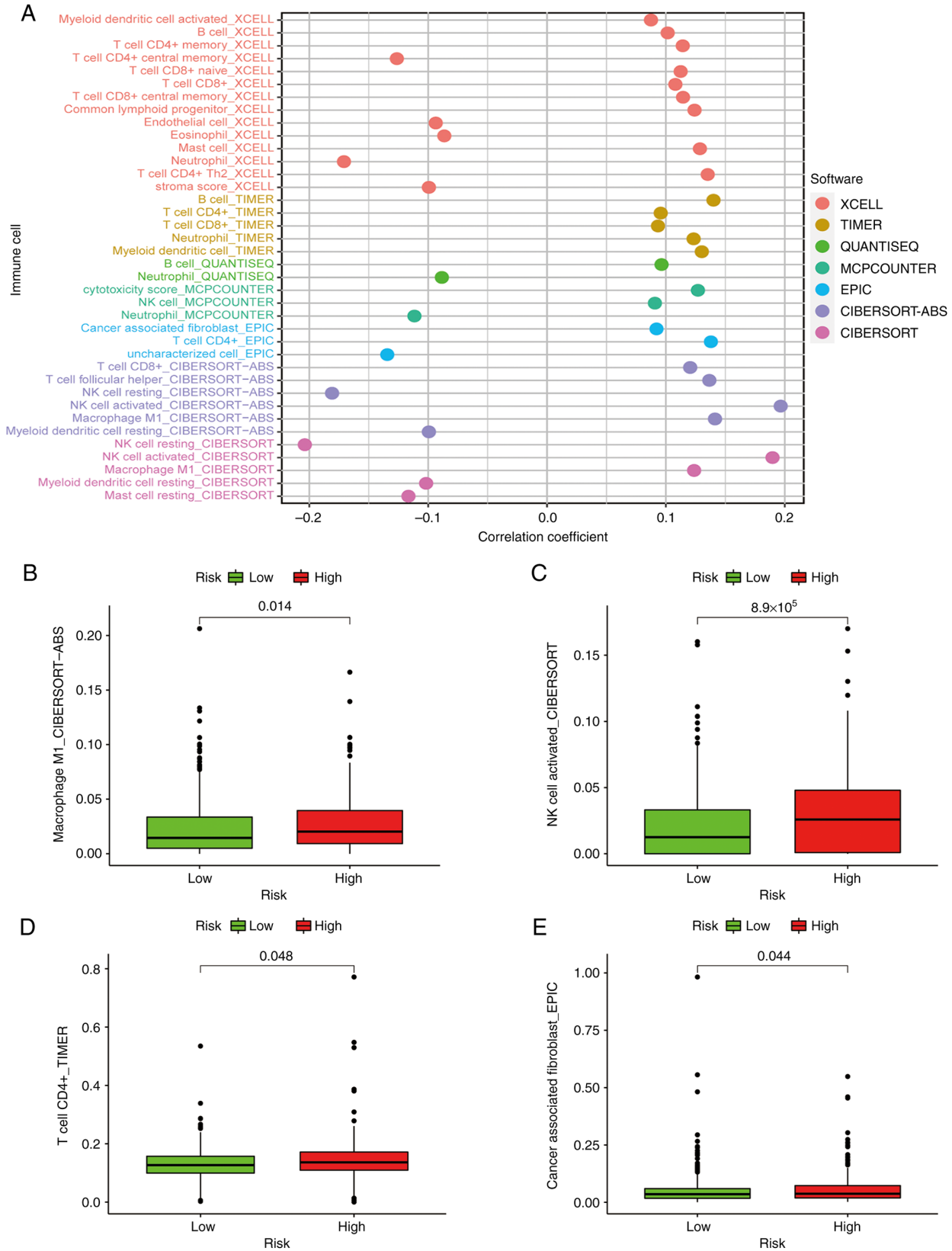

Figure 8. Analysis of immune cell infiltration based on risk score. (A) Lollipop chart displaying the correlation coefficients of infiltrating immune cells from multiple databases. The correlation coefficient reflects the relationship between the quantity of immune cells and patients' risk score. High-risk was positively associated with (B) macrophages, (C) NK cells, (D) $CD4^+$ T cells and (E) cancer-associated fibroblasts.

In the present study, all orgenes were collected by first searching the oncosis-related literature, followed by obtaining the original transcriptome CRC data from the TCGA database. The Wilcoxon signed-rank test and other testing methods were used for analyzing co-expression and differential expression to recognize DEorlncRNAs. The contributing DEorlncRNA

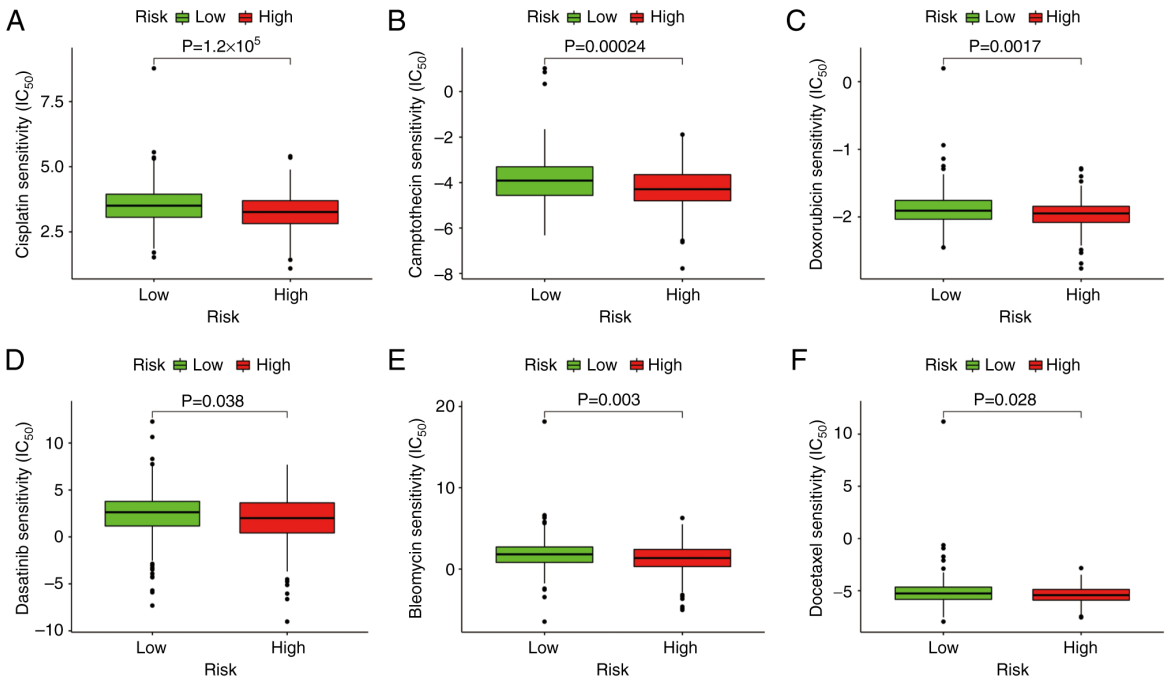

Figure 9. Evaluation of the risk model for different chemotherapy drugs. The box plots suggested that patients with high-risk scores had a lower IC_{50} for (A) cisplatin (P=1.2x10^{-5}), (B) camptothecin (P=0.00024), (C) doxorubicin (P=0.0017), (D) dasatinib (P=0.038), (E) bleomycin (P=0.003) and (F) docetaxel (P=0.028). The dots represented outliers, the bar indicated the limits of the non-abnormal data.

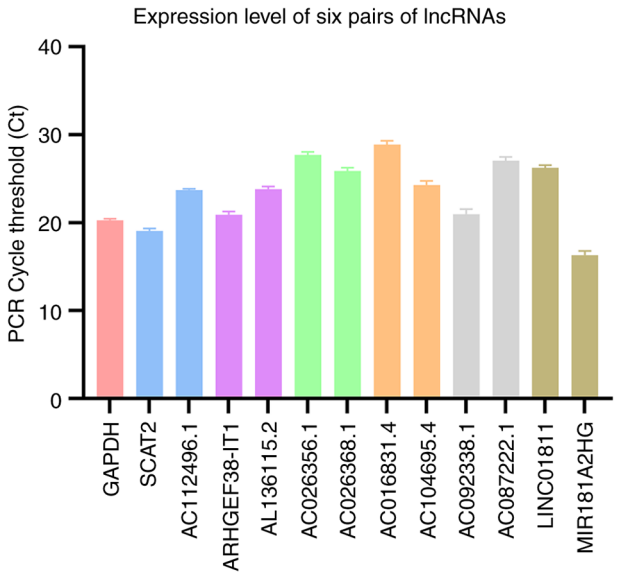

Figure 10. Expression level of six pairs of lncRNAs. The bar graph indicates that the expression levels of SCAT2, ARHGEF38-IT1, AC026368.1, AC104695.4, AC092338.1 and MIR181A2HG were markedly higher in the corresponding lncRNA pairs. lncRNA, long noncoding RNA.

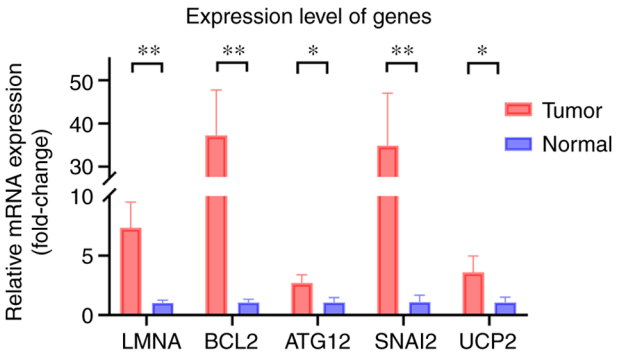

Figure 11. Expression level of genes in tumor and normal tissue. Bar graph indicating that the expression level of LMNA, BCL2, ATG12, SNAI2 and UCP2 was higher in tumor tissue than in normal tissue (GAPDH was used as the reference for normalization). *P<0.05 and **P<0.01.

pairs were verified by circular pairing and a 0-or-1 matrix. The DEorlncRNA pairs included in the model were determined through a series of analyses, including Lasso and Cox regression analyses. The AIC value was determined to recognize the optimal model and the sum of sensitivity and specificity of each point on the 1-, 3- and 5-year ROC curves were calculated to find the optimal risk score cut-off. The model was validated using case data and further evaluated in terms of survival time, clinicopathological progression, related gene expression, infiltration of immune cells into the tumor and sensitivity to chemotherapy. Based on the model, it was observed that the prognosis of patients in the high-risk group significantly differed from that of the low-risk group and the survival outcome of patients in the high-risk group was significantly worse than that in the low-risk group. The risk score of patients was related to tumor-node-metastasis (TNM) and clinical stage, with a higher risk score associated with a higher TNM and clinical stage. Certain genes exhibited a higher level of expression in the high-risk group than in the low-risk group (e.g., ATG12, BCL2, LMNA, UCP2 and SNAI2), whereas the opposite was observed for the NDRG2 gene. Such gene expression status changes may provide supporting evidence for cancer prognosis. ATG12 deficiency leads to depletion of intracellular levels of L-glutamine, which is associated with a lower tolerance to hypoxia and an improved cancer

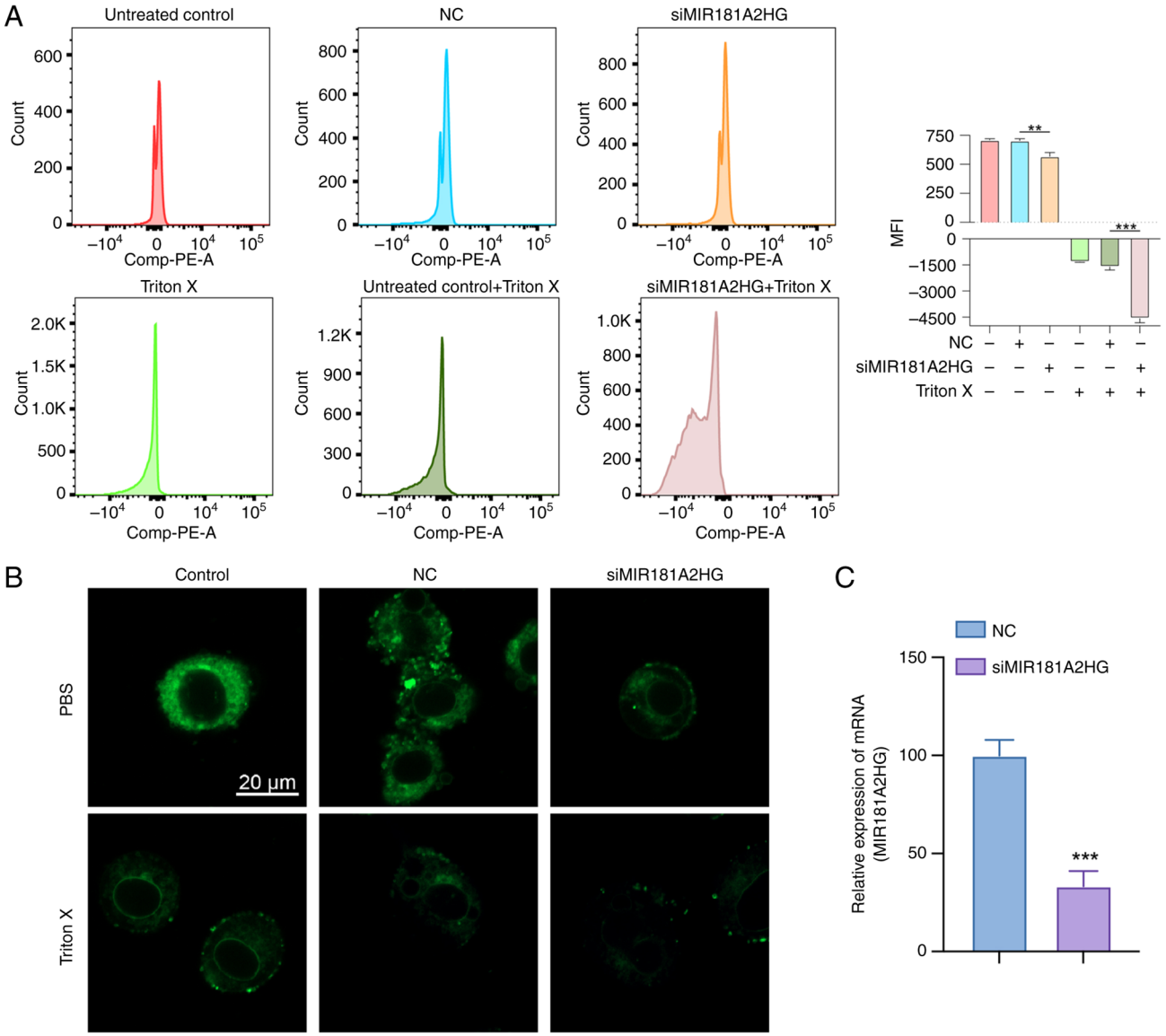

Figure 12. Biological impact of the MIR181A2HG. (A) Data detected using flow tcytometry and DilC1(5). As shown in the figure, The histogram groups are (a) untreated control, (b) NC, (c) siMIR181A2HG, (d) Triton X only control, (e)Triton X-NC, (f) Triton X-siMIR181A2HG, from left to right. (B) Fluorescence confocal microscopy of LoVo cells labeled with DilC1(5) (scale bar, 20 μm). (C) siRNA transfection efficiency was verified. **P<0.01 and ***P<0.001. MFI (mean fluorescence intensity); NC, negative control (cells transfected with si-NC); si, small interfering RNA; miR, microRNA.

prognosis (41). Furthermore, ATG12 silencing in CRC may weaken cell viability, induce cell apoptosis, inhibit autophagy and enhance the radiosensitivity of CRC cells. BCL2, a known antiapoptotic protein, may inhibit apoptosis by reducing the level of activated caspase (42). Inhibition of BCL2 may therefore promote apoptosis of CRC cells (43). Metastatic tumors of the prostate are highly aggressive, have a slow proliferation rate and exhibit elevated SNAI2 expression (44). Certain studies have found that increased SNAI2 expression was associated with CRC cell invasion (45,46). The NTRK1-LMNA axis may be associated with extensive phenotypic changes in neuroblastoma cells and NTRK1-induced reprogramming (47). LMNA is also expressed in colon stem cells and, statistically, the prognosis of patients with an LMNA-positive tumor is significantly worse than that of patients with an LMNA-negative tumor (48). In addition, UCP2 has been indicated to have different roles according to cell type and the regulation of its expression is correlated with the progression and treatment of cancer cells (49). UCP2 has a key role in the mitochondrial apoptosis pathway and inhibition of UCP2 promotes apoptosis in CRC cells. Furthermore, in murine intestinal cancer models and samples from patients with CRC, higher levels of UCP2 protein were observed than in non-tumor counterparts (50,51). Functioning as either a tumor suppressor gene or stress response gene, NDRG2 has been associated with antimetastasis and antiproliferation responses in tumors and the level of NDRG2 expression is related to tumor prognosis (52). Since oncosis is related to the immune response (53,54), a number of methods were used in the present study to comprehensively evaluate infiltrating immune cells in CRC. According to the analysis, cancer-associated fibroblasts, NK cells, $CD4^+$ T cells and macrophage content were higher in the high-risk group in the present model. A previous study has indicated that the metastatic potential of ovarian cancer cells may be increased

Table II. Results of the correlation between tumor-infiltrating immune cells and risk score.

Symbol	Spearman correlation coefficient	P-value
B cell_TIMER	0.140020872	0.001444718
T cell CD4+_TIMER	0.095646701	0.029986209
T cell CD8+_TIMER	0.093339716	0.034201057
Neutrophil_TIMER	0.123325136	0.005069284
Myeloid dendritic cell_TIMER	0.130194203	0.003076337
NK cell resting_CIBERSORT	-0.20379316	$3.12x10^{-6}$
NK cell activated_CIBERSORT	0.189706121	$1.46x10^{-5}$
Macrophage M1_CIBERSORT	0.123725861	0.004926897
Myeloid dendritic cell resting_CIBERSORT	-0.101734416	0.020937744
Mast cell resting_CIBERSORT	-0.116602694	0.008079078
T cell CD8+_CIBERSORT-ABS	0.120419134	0.006217829
T cell follicular helper_CIBERSORT-ABS	0.136542775	0.001898442
NK cell resting_CIBERSORT-ABS	-0.180865302	$3.65x10^{-5}$
NK cell activated_CIBERSORT-ABS	0.196574724	$6.99x10^{-6}$
Macrophage M1_CIBERSORT-ABS	0.141280063	0.001306712
Myeloid dendritic cell resting_CIBERSORT-ABS	-0.099423856	0.024045776
B cell_QUANTISEQ	0.096337307	0.028814455
Neutrophil_QUANTISEQ	-0.088510252	0.044677492
cytotoxicity score_MCPCOUNTER	0.126957411	0.003904117
NK cell_MCPCOUNTER	0.090727199	0.039573709
Neutrophil_MCPCOUNTER	-0.111578196	0.011280863
Myeloid dendritic cell activated_XCELL	0.087432741	0.047351518
B cell_XCELL	0.101477075	0.021265689
T cell CD4+ memory_XCELL	0.114174225	0.009508347
T cell CD4+ central memory_XCELL	-0.126344576	0.004081879
T cell CD8+ naive_XCELL	0.112402483	0.010688716
T cell CD8+_XCELL	0.1079606	0.014236864
T cell CD8+ central memory_XCELL	0.114425918	0.009350425
Common lymphoid progenitor_XCELL	0.124081452	0.004803578
Endothelial cell_XCELL	-0.09362572	0.033652529
Eosinophil_XCELL	-0.086455384	0.049891825
Mast cell_XCELL	0.128617222	0.003457318
Neutrophil_XCELL	-0.17086684	$9.74x10^{-5}$
T cell CD4+ Th2_XCELL	0.135172714	0.00211051
stroma score_XCELL	-0.099411962	0.024062755
Cancer associated fibroblast_EPIC	0.092110535	0.036646054
T cell CD4+_EPIC	0.137868277	0.00171202

NK, natural killer; Th2, type 2 T-helper.

by pro-inflammatory M1 macrophages through activation of the NF-κB signaling pathway (55). According to the risk model in the present study, the drug sensitivity results indicated that patients in the high-risk group treated with bleomycin, camptothecin, tipifarnib, dasatinib, docetaxel, doxorubicin or cisplatin tended to have a higher tumor mutation burden (TMB).

In the six DeorlncRNA pairs included in the Lasso regression analysis, at least three of the orlncRNAs described below were demonstrated to be associated with cancer progression. LncRNA MIR181A2HG inhibits the proliferation, migration and capillary-like structures of vascular endothelial cells through dysregulation of the miRNAs/AKT2 axis (56). Another study demonstrated that MIR181A2HG is a prognostic predictor of bladder cancer survival time and is an immune checkpoint inhibitor (57). The MIR181A2HG gene is also overexpressed in the thyroid and there is a connection between MIR181A2HG and the prognosis of thyroid cancer (58,59). In addition, LncRNA AC104695.4 as a component of the prediction model, is positively correlated with

TGFβ1 expression in triple negative breast cancer tissue (60). LncRNA ARHGEF38-IT1 was significantly associated with the survival time, clinical features, immune cells in the tumor microenvironment, TMB and cancer-related pathways of stomach adenocarcinoma (61). In the present study, an early-stage CRC tissue sample was selected and the expression of six pairs of lncRNA were verified by RT-qPCR. The results indicated that the sample was in the low-risk group and consistent with clinical diagnosis. To further improve the credibility of the algorithm, a lncRNA was randomly selected and the biological process in oncosis was verified. Flow cytometry and fluorescence confocal microscopy results indicated that knockdown of MIR181A2HG expression promoted the oncosis of LoVo cells, which indicated MIR181A2HG was associated with oncosis. All the aforementioned studies verified the validation of the algorithm. The remaining DEorlncRNAs were reported in the present study for the first time and require further exploration and research.

In the present study, a novel algorithm based on oncosis was established to explore the clinical implications of risk assessment models. The algorithm indicated that DEorLncRNAs may be identified and associated vital pairs may be constructed. The AUC values of the 1-, 3- and 5-year ROC curves of the model were all >0.7, exhibiting a fair predictive performance. There have been multiple studies on the establishment of lncRNA-related prediction models for CRC and each algorithm have their own advantages, such as using simple predictors, and disadvantages, such as insufficient clinical and molecular biological validation (62,63). In the present study, orlncRNAs were applied for the construction of the CRC prediction model for the first time and differential orlncRNAs were identified to form DEorlncRNA pairs. The study models used by others frequently require the batch correction of clinical data. Thus, since the present model uses DEorlncRNA pairs, only the expression levels of the lncRNA pairs require to be compared, thereby avoiding the need for data correction. Therefore, there is a substantially lower threshold for the clinical application of this model and errors related to differences in the detection of marker expression are largely avoided.

There are certain limitations to the present study. First, since the data were obtained from open public databases, the sample size may be relatively small and there may be certain bias in the analyzed profile. Furthermore, the data in the TCGA database were used to internally verify the constructed risk assessment model, but it should also be externally verified. In addition, the correlation between the model and immune cell features requires to be verified by clinical data and other experiments. Finally, the new algorithm ultimately serves clinical treatment and in future clinical work, our clinical case validation of this model is insufficient since only one sample was verified by PCR and there is a requirement to collect additional samples to verify the predictive ability of this algorithm for the clinical treatment of patients with CRC.

In summary, the present study successfully established a new algorithm consisting of paired orlncRNAs in CRC and the algorithm was verified to a certain extent. Only the expression levels of six lncRNA pairs needed to be detected and compared to divide CRC patients into high- and low-risk groups and to predict their survival outcomes, related tumor immune cell infiltration and sensitivity to drug treatment. The model may provide individualized management and treatment for patients with CRC.

Acknowledgements

Not applicable.

Funding

This study was supported by the National Natural Science Foundation of China (grant no. 82002982).

Availability of data and materials

The datasets used and/or analyzed during the current study are available from the corresponding authors on reasonable request.

Authors' contributions

ZS and WC conceptualized the study. HX and XS performed the experiments and acquired the data. HX, XS and EC were involved in data analysis, writing and preparation of the original draft. EC was involved in the writing, reviewing and editing of the manuscript. All authors read and approved the final version of the manuscript. ZS, WC, HX, EC and XS confirm the authenticity of all the raw data.

Ethics approval and consent to participate

All patients and healthy donors signed the written informed consent form. All experiments involving patient tissue were approved by the Medical Ethics Committee of Sir Run Run Shaw Hospital affiliated to Zhejiang University School of Medicine (Hangzhou, China; approval no. 20211108-31) and were conducted according to the Ethical Review Measures for Biomedical Research involving People (2016) of the National Health Commission. The tissue experiments involving human participants complied with the Declaration of Helsinki.

Patient consent for publication

Not applicable.

Competing interests

The authors declare that they have no competing interests.

References

1. Sung H, Ferlay J, Siegel RL, Laversanne M, Soerjomataram I, Jemal A and Bray F: Global cancer statistics 2020: GLOBOCAN estimates of incidence and mortality worldwide for 36 cancers in 185 countries. CA Cancer J Clin 71: 209-249, 2021.
2. Bray F, Ferlay J, Soerjomataram I, Siegel RL, Torre LA and Jemal A: Global cancer statistics 2018: GLOBOCAN estimates of incidence and mortality worldwide for 36 cancers in 185 countries. CA Cancer J Clin 68: 394-424, 2018.
3. Dekker E, Tanis P, Vleugels J, Kasi P and Wallace M: Colorectal cancer. Lancet 394: 1467-1480, 2019.
4. Weerasinghe P and Buja LM: Oncosis: An important non-apoptotic mode of cell death. Exp Mol Pathol 93: 302-308, 2012.
5. Trump BF and Berezesky IK: Calcium-mediated cell injury and cell death. FASEB J 9: 219-228, 1995.

6. Peters AA, Jamaludin SYN, Yapa KTDS, Chalmers S, Wiegmans AP, Lim HF, Milevskiy MJG, Azimi I, Davis FM, Northwood KS, *et al*: Oncosis and apoptosis induction by activation of an overexpressed ion channel in breast cancer cells. Oncogene 36: 6490-6500, 2017.
7. Mills EM, Xu D, Fergusson MM, Combs CA, Xu Y and Finkel T: Regulation of cellular oncosis by uncoupling protein 2. J Biol Chem 277: 27385-27392, 2002.
8. Majno G and Joris I: Apoptosis, oncosis, and necrosis. An overview of cell death. Am J Pathol 146: 3-15, 1995.
9. Wang L, Mai Z, Zhao M, Wang B, Yu S, Wang X and Chen T: Aspirin induces oncosis in tumor cells. Apoptosis 24: 758-772, 2019.
10. Guan R, Chen Y, Zeng L, Rees TW, Jin C, Huang J, Chen ZS, Ji L and Chao H: Oncosis-inducing cyclometalated iridium(iii) complexes. Chem Sci 9: 5183-5190, 2018.
11. Derrien T, Johnson R, Bussotti G, Tanzer A, Djebali S, Tilgner H, Guernec G, Martin D, Merkel A, Knowles DG, *et al*: The GENCODE v7 catalog of human long noncoding RNAs: Analysis of their gene structure, evolution, and expression. Genome Res 22: 1775-1789, 2012.
12. Okugawa Y, Toiyama Y, Hur K, Toden S, Saigusa S, Tanaka K, Inoue Y, Mohri Y, Kusunoki M, Boland CR and Goel A: Metastasis-associated long non-coding RNA drives gastric cancer development and promotes peritoneal metastasis. Carcinogenesis 35: 2731-2739, 2014.
13. Schmitt AM and Chang HY: Gene regulation: Long RNAs wire up cancer growth. Nature 500: 536-537, 2013.
14. Schmidt LH, Spieker T, Koschmieder S, Schäffers S, Humberg J, Jungen D, Bulk E, Hascher A, Wittmer D, Marra A, *et al*: The long noncoding MALAT-1 RNA indicates a poor prognosis in non-small cell lung cancer and induces migration and tumor growth. J Thorac Oncol 6: 1984-1992, 2011.
15. Yan X, Hu Z, Feng Y, Hu X, Yuan J, Zhao SD, Zhang Y, Yang L, Shan W, He Q, *et al*: Comprehensive genomic characterization of long non-coding RNAs across human cancers. Cancer Cell 28: 529-540, 2015.
16. Matsumura H, Shimizu Y, Ohsawa Y, Kawahara A, Uchiyama Y and Nagata S: Necrotic death pathway in Fas receptor signaling. J Cell Biol 151: 1247-1256, 2000.
17. Holler N, Zaru R, Micheau O, Thome M, Attinger A, Valitutti S, Bodmer JL, Schneider P, Seed B and Tschopp J: Fas triggers an alternative, caspase-8-independent cell death pathway using the kinase RIP as effector molecule. Nat Immunol 1: 489-495, 2000.
18. Tanabe K, Nakanishi H, Maeda H, Nishioku T, Hashimoto K, Liou SY, Akamine A and Yamamoto K: A predominant apoptotic death pathway of neuronal PC12 cells induced by activated microglia is displaced by a non-apoptotic death pathway following blockage of caspase-3-dependent cascade. J Biol Chem 274: 15725-15731, 1999.
19. Akimoto M, Hayashi JI, Nakae S, Saito H and Takenaga K: Interleukin-33 enhances programmed oncosis of ST2L-positive low-metastatic cells in the tumour microenvironment of lung cancer. Cell Death Dis 7: e2057, 2016.
20. Chen YG, Satpathy AT and Chang HY: Gene regulation in the immune system by long noncoding RNAs. Nat Immunol 18: 962-972, 2017.
21. Li Y, Jiang T, Zhou W, Li J, Li X, Wang Q, Jin X, Yin J, Chen L, Zhang Y, *et al*: Pan-cancer characterization of immune-related lncRNAs identifies potential oncogenic biomarkers. Nat Commun 11: 1000, 2020.
22. Fang T, Liang T, Wang Y, Wu H, Liu S, Xie L, Zhang Z, Liang J, Yao C, Tan Y and Wang C: An early-onset advanced rectal cancer patient with increased KRAS gene copy number showed A primary resistance to cetuximab in combination with chemotherapy: A case report. Front Oncol 11: 755578, 2021.
23. Lv Y, Lin SY, Hu FF, Ye Z, Zhang Q, Wang Y and Guo AY: Landscape of cancer diagnostic biomarkers from specifically expressed genes. Brief Bioinform 21: 2175-2184, 2020.
24. Tomczak K, Czerwinska P and Wiznerowicz M: The cancer genome atlas (TCGA): An immeasurable source of knowledge. Contemp Oncol (Pozn) 19: A68-A77, 2015.
25. Fiorini N, Lipman DJ and Lu Z: Towards PubMed 2.0. Elife 6: e28801, 2017.
26. Ritchie ME, Phipson B, Wu D, Hu Y, Law CW, Shi W and Smyth GK: limma powers differential expression analyses for RNA-sequencing and microarray studies. Nucleic Acids Res 43: e47, 2015.
27. Akaike H: A new look at the statistical model identification. IEEE Trans Automat Contr AC 19: 716-723, 1974.
28. Amin MB, Greene FL, Edge SB, Compton CC, Gershenwald JE, Brookland RK, Meyer L, Gress DM, Byrd DR and Winchester DP: The eighth edition AJCC cancer staging manual: Continuing to build a bridge from a population-based to a more 'personalized' approach to cancer staging. CA Cancer J Clin 67: 93-99, 2017.
29. Strutner J, Ramchandar N, Dubey S, Gamboa M, Vanderpool MK, Mueller T, Wang W, Cannavino C, Tovar Padua L, Malicki D and Pong A: Comparison of RT-PCR cycle threshold values from respiratory specimens in symptomatic and asymptomatic children with SARS-CoV-2 infection. Clin Infect Dis: ciab403, 2021 (Epub ahead of print).
30. Chen Y, Lu B, Yang Q, Fearns C, Yates JR III and Lee JD: Combined integrin phosphoproteomic analyses and small interfering RNA-based functional screening identify key regulators for cancer cell adhesion and migration. Cancer Res 69: 3713-3720, 2009.
31. Warnes G and Martins S: Real-time flow cytometry for the kinetic analysis of oncosis. Cytometry A 79: 181-191, 2011.
32. D'Arcy MS: Cell death: A review of the major forms of apoptosis, necrosis and autophagy. Cell Biol Int 43: 582-592, 2019.
33. Luo D, Ni Q, Ji A, Gu W, Wu J and Jiang C: Dehydroabietic acid derivative QC4 induces gastric cancer cell death via oncosis and apoptosis. Biomed Res Int 2016: 2581061, 2016.
34. Huarte M: The emerging role of lncRNAs in cancer. Nat Med 21: 1253-1261, 2015.
35. Zhang W, Fang D, Li S, Bao X, Jiang L and Sun X: Construction and validation of a novel ferroptosis-related lncRNA signature to predict prognosis in colorectal cancer patients. Front Genet 12: 709329, 2021.
36. Yu J, Mao W, Xu B and Chen M: Construction and validation of an autophagy-related long noncoding RNA signature for prognosis prediction in kidney renal clear cell carcinoma patients. Cancer Med 10: 2359-2369, 2021.
37. Ghafouri-Fard S and Taheri M: Long non-coding RNA signature in gastric cancer. Exp Mol Pathol 113: 104365, 2020.
38. Liu S, Cao Q, An G, Yan B and Lei L: Identification of the 3-lncRNA signature as a prognostic biomarker for colorectal cancer. Int J Mol Sci 21: 9359, 2020.
39. Wei J, Ge X, Tang Y, Qian Y, Lu W, Jiang K, Fang Y, Hwang M, Fu D, Xiao Q and Ding K: An autophagy-related long noncoding RNA signature contributes to poor prognosis in colorectal cancer. J Oncol 2020: 4728947, 2020.
40. Tang R, Wu Z, Rong Z, Xu J, Wang W, Zhang B, Yu X and Shi S: Ferroptosis-related lncRNA pairs to predict the clinical outcome and molecular characteristics of pancreatic ductal adenocarcinoma. Brief Bioinform 23: bbab388, 2022.
41. Keulers TG, Koch A, van Gisbergen MW, Barbeau LMO, Zonneveld MI, de Jong MC, Savelkouls KGM, Wanders RG, Bussink J, Melotte V and Rouschop KMA: ATG12 deficiency results in intracellular glutamine depletion, abrogation of tumor hypoxia and a favorable prognosis in cancer. Autophagy 18: 1898-1914, 2022.
42. Llambi F, Wang YM, Victor B, Yang M, Schneider DM, Gingras S, Parsons MJ, Zheng JH, Brown SA, Pelletier S, *et al*: BOK is a non-canonical BCL-2 family effector of apoptosis regulated by ER-associated degradation. Cell 165: 421-433, 2016.
43. Dai W, Mu L, Cui Y, Li Y, Chen P, Xie H and Wang X: Long non-coding RNA CASC2 enhances berberine-induced cytotoxicity in colorectal cancer cells by silencing BCL2. Mol Med Rep 20: 995-1006, 2019.
44. Mazzu YZ, Liao Y, Nandakumar S, Sjöström M, Jehane LE, Ghale R, Govindarajan B, Gerke TA, Lee GM, Luo JH, *et al*: Dynamic expression of SNAI2 in prostate cancer predicts tumor progression and drug sensitivity. Mol Oncol 16: 2451-2469, 2022.
45. Findlay VJ, Wang C, Nogueira LM, Hurst K, Quirk D, Ethier SP, Staveley O'Carroll KF, Watson DK and Camp ER: SNAI2 modulates colorectal cancer 5-fluorouracil sensitivity through miR145 repression. Mol Cancer Ther 13: 2713-2726, 2014.
46. Du F, Li X, Feng W, Qiao C, Chen J, Jiang M, Qiu Z, Qian M, Tian D, Nie Y, *et al*: SOX13 promotes colorectal cancer metastasis by transactivating SNAI2 and c-MET. Oncogene 39: 3522-3540, 2020.
47. Funke L, Bracht T, Oeck S, Schork K, Stepath M, Dreesmann S, Eisenacher M, Sitek B and Schramm A: NTRK1/TrkA signaling in neuroblastoma cells induces nuclear reorganization and intra-nuclear aggregation of lamin A/C. Cancers (Basel) 13: 5293, 2021.
48. Willis ND, Cox TR, Rahman-Casañs SF, Smits K, Przyborski SA, van den Brandt P, van Engeland M, Weijenberg M, Wilson RG, de Bruïne A and Hutchison CJ: Lamin A/C is a risk biomarker in colorectal cancer. PLoS One 3: e2988, 2008.

49. Kim DY, Cheong HT, Ra CS, Kimura K and Jung BD: Effect of 5-azacytidine (5-aza) on UCP2 expression in human liver and colon cancer cells. Int J Med Sci 18: 2176-2186, 2021.
50. Aguilar E, Esteves P, Sancerni T, Lenoir V, Aparicio T, Bouillaud F, Dentin R, Prip-Buus C, Ricquier D, Pecqueur C, *et al*: UCP2 deficiency increases colon tumorigenesis by promoting lipid synthesis and depleting NADPH for antioxidant defenses. Cell Rep 28: 2306-2316.e5, 2019.
51. Qiao C, Wei L, Dai Q, Zhou Y, Yin Q, Li Z, Xiao Y, Guo Q and Lu N: UCP2-related mitochondrial pathway participates in oroxylin A-induced apoptosis in human colon cancer cells. J Cell Physiol 230: 1054-1063, 2015.
52. Kim G, Lim S and Kim KD: N-myc downstream-regulated gene 2 (NDRG2) function as a positive regulator of apoptosis: A new insight into NDRG2 as a tumor suppressor. Cells 10: 2649, 2021.
53. Moreno E and Barquero-Calvo E: The role of neutrophils in brucellosis. Microbiol Mol Biol Rev 84: e00048-20, 2020.
54. Davidson WF, Haudenschild C, Kwon J and Williams MS: T cell receptor ligation triggers novel nonapoptotic cell death pathways that are Fas-independent or Fas-dependent. J Immunol 169: 6218-6230, 2002.
55. Cho U, Kim B, Kim S, Han Y and Song YS: Pro-inflammatory M1 macrophage enhances metastatic potential of ovarian cancer cells through NF-κB activation. Mol Carcinog 57: 235-242, 2018.
56. Wang S, Zheng B, Zhao H, Li Y, Zhang X and Wen J: Downregulation of lncRNA MIR181A2HG by high glucose impairs vascular endothelial cell proliferation and migration through the dysregulation of the miRNAs/AKT2 axis. Int J Mol Med 47: 35, 2021.
57. Wu Y, Zhang L, He S, Guan B, He A, Yang K, Gong Y, Li X and Zhou L: Identification of immune-related LncRNA for predicting prognosis and immunotherapeutic response in bladder cancer. Aging (Albany NY) 12: 23306-23325, 2020.
58. Yang F, Zhang J, Li B, Zhao Z, Liu Y, Zhao Z, Jing S and Wang G: Identification of potential lncRNAs and miRNAs as diagnostic biomarkers for papillary thyroid carcinoma based on machine learning. Int J Endocrinol 2021: 3984463, 2021.
59. Xu Y, Chen J, Yang Z and Xu L: Identification of RNA expression profiles in thyroid cancer to construct a competing endogenous RNA (ceRNA) network of mRNAs, long noncoding RNAs (lncRNAs), and microRNAs (miRNAs). Med Sci Monit 25: 1140-1154, 2019.
60. Vishnubalaji R and Alajez NM: Epigenetic regulation of triple negative breast cancer (TNBC) by TGF-β signaling. Sci Rep 11: 15410, 2021.
61. Ye Z, Zheng M, Zeng Y, Wei S, Wang Y, Lin Z, Shu C, Xie Y, Zheng Q and Chen L: Bioinformatics analysis reveals an association between cancer cell stemness, gene mutations, and the immune microenvironment in stomach adenocarcinoma. Front Genet 11: 595477, 2020.
62. Liu Z, Liu L, Weng S, Guo C, Dang Q, Xu H, Wang L, Lu T, Zhang Y, Sun Z and Han X: Machine learning-based integration develops an immune-derived lncRNA signature for improving outcomes in colorectal cancer. Nat Commun 13: 816, 2022.
63. Song W, Ren J, Yuan W, Xiang R, Ge Y and Fu T: N6-methyladenosine-related lncRNA signature predicts the overall survival of colorectal cancer patients. Genes (Basel) 12: 1375, 2021.